Journal of Telecommunication, Electronic and Computer Engineering
ISSN: 2180 – 1843 e-ISSN: 2289-8131 Vol. 18 No. 2 (2026) 35-44
jtec.utem.edu.my
DOI: https://doi.org/10.54554/jtec.2026.18.02.005

Alternative Signal Waveform Models for Advanced Interference Mitigation in 5G New Radio Systems

Zakka Augustine[1*], Gambo Danasabe[2], Franklin Chibueze Njoku[1], Jerry Raymond[1], Magaji Musa Marcus[3], Stella Ngozi Obiahu[4]
[1]*Department of Telecommunications Engineering, Faculty of Ground Engineering, Air Force Institute of Technology, Kaduna 800282, Nigeria.*
[2] *Department of Electrical Electronics Engineering, Faculty of Ground Engineering, Air Force Institute of Technology, Kaduna, Nigeria.*
[3] *Department of Cyber Security, Faculty of Computing, Federal University of Applied Sciences, Kachia, Nigeria.*
[4] *Department of Control Engineering, Faculty of Engineering, Ahmadu Bello University, Zaria, Nigeria.*

Article Info
Article history:
Received Mar 14th, 2026
Revised May 6th, 2026
Accepted Jun 3rd, 2026
Published Jun 30th, 2026

Index Terms:
Adjacent Channel Interference, Advanced Interference Mitigation, Closed Loop Transfer Function, Inter-Channel Interference, Inter-Symbol Interference

Abstract
The need for alternative signal waveforms that could amicably mitigate interference and increase transmission efficiency has been a challenge posed for Fifth Generation (5G) New Radio (NR) systems frequencies. With this in mind, this research developed two modified waveforms using Kaiser Windowed (KW) and Dolph-Chebyshev Windowed (DW) algorithms in a programmable Closed Loop Transfer Function (CLTF) digital module paired in a Hanning Windowed (HW)-induced Filtered-Orthogonal Frequency Division Multiplexing (F-OFDM) model. This formed two alternative waveforms: Hann-Kaiser Windowed F-OFDM (HKW-FOFDM) and Hann-Dolph Windowed F-OFDM (HDW-FOFDM). Simulation results taken at 120 kHz Subcarrier Spacing (SCS) showed the HKW-FOFDM system obtained an Advanced Interference Mitigation (AIM) of -25.22 dBm for Adjacent Channel Interference (ACI), -40.05 dBm for Inter-Symbol Interference (ISI), and -53.70 dBm for Inter-Channel Interference (ICI), which amounted to an improvement of 22.73%, 24.84%, and 28.49% over those obtained by the HW-FOFDM system, respectively. Similarly, the HDW-FOFDM achieved an AIM of -30.02 dBm for ACI, -38.52 dBm for ISI, and -51.17 dBm for ICI, which resulted in an improvement of 46.08%, 20.07%, and 22.44% over those obtained by the HW-FOFDM system, respectively. The two modified waveforms have the added advantage of increasing bandwidth and spectra gain that meets the extreme demands for Frequency Two (FR2/mmWave) deployments ($> 24.25\ GHz$) by virtue of AIM. This is proven in its scalability to efficiently drive varying 5G NR numerologies of 0 to 3.

*Corresponding Author: zax.austen@yahoo.com

I. INTRODUCTION

Filtering/windowing of signals is one of the key performance indicators required to achieve maximum Spectral Efficiency (SE) in wireless waveform modification [1]. It is mostly used to sufficiently mitigate interference and attain asynchronicity as postulated by the Third Generation Partnership Project (3GPP) Fifth Generation (5G) New Radio (NR) objectives. An interference anomaly usually causes underutilization of the radio wave resources [2]. To efficiently achieve spectral filtering for Advanced Interference Mitigation (AIM), this research adopted the use of augmented filter response. Digital filters are used to discriminate a frequency or bands of frequencies from a given signal, which is normally a mixture of wanted and unwanted signals [3, 4]. The unwanted signals could be as a result of interference or noise, which normally results to an unhealthy condition that obstructs various applications in wireless transmission [5]. There are two broad types of window-induced digital filters mostly used for waveform development, known as: Finite Impulse Response (FIR) and Infinite Impulse Response (IIR) [6]. This research focuses on the use of the FIR filter function (Windowed-Sinc filter) to modify a Filtered-Orthogonal Frequency Division Multiplexing (F-OFDM) waveform. F-OFDM is an Orthogonal Multiple Access (OMA) scheme proposed for future fifth-generation (5G) telecommunications to meet the demand for massive connectivity and flexible spectra mapping on sub-band filtering [7]. Unlike the Non-Orthogonal Multiple Access (NOMA) that focuses on energy utilization, the OMA uses spectral frequency, time, and code for its SE [8]. This is to achieve an alternative and an advanced signal waveform that mitigates interference in 5G NR systems. The F-OFDM is known for the limitation of reintroducing Adjacent Channel Interference (ACI), Inter-Channel Interference (ICI), and Inter-Symbol Interference

(ISI) after the removal of the Cyclic Prefix (CP) at the receiver side of a wireless transceiver [9]. This proposed AIM is achieved by the systematic design/introduction of a programmable Closed Loop Transfer Function (CLTF) system placed in an F-OFDM receiver to curtail its limitations. The CLTF improved module is synonymous with the system design of the Cyclic Prefix-Orthogonal Frequency Division Multiplexing (CP-OFDM) method for Interference Mitigation (IM), where a percentage of each suffix information is copied and duplicated at the prefix in the CP-OFDM [10]. This is the simple logic that makes CP-OFDM one of the best systems for interference/noise control, if not for its inherent waste of bandwidth, which results in time wastage and increased power consumption [11, 12]. The CP-OFDM is known to offer many benefits, including its robustness against multipath transmission and relatively low sensitivity to timing [13, 14]. In this like manner, the unwanted bit codes observed are extracted from the channel estimation region of a Hanning Windowed (HW) F-OFDM receiver and referred to the Kaiser Windowed (KW) and/or Dolph Windowed (DW) filters' alternate region in the CLTF module. This is to be postfiltered using the digital FIR filter capability of interference control. After the mitigation of interference to a wanted threshold using the adaptive KW-induced or DW-induced filters with the aid of the programmable CLTF model features, the obtained filtered signal is backed up perpendicularly to the input section of the receiver. It is backed up in order to complement any noticeable error signal pulses and also to provide the required timing to adequately curtail ACI, ICI, and ISI distortions. Finally, the certified waveforms are passed through the channel estimation region to be demodulated as waveforms that fall within the threshold of the wanted signal requirement. This method is to enable efficient network slicing as required for 5G NR and beyond [2]. In this work, the newly modified waveforms are targeted to be deployed to explore and exploit 60 kHz and 120 kHz Subcarrier Spacings (SCS) of 5G numerologies and beyond. This is aimed at achieving a transmission range within the bands of 24.52 GHz – 52.60 GHz earmarked for 5G Frequency Two (FR2) [15]. Experimental activities indicate that higher SCS values enable more efficient data transmission [16]. For example, the smartphones have low jittery symmetry within numerology values of 2 and 3, making them well-suited for bidirectional communication [17]. This need for higher SCS to mitigate interference also results in network redundancies. The Software Defined Radio (SDR) technique of Cognitive Radio (CR) and Machine Learning (ML) algorithms are proposed as a promising technique that could maximize the utilization of these redundant spectra and improve system scalability [18]. This is one of the key significant recommendations of this work in order to meet the 3GPP 5G NR requirement for increasing data rates.

The novelty of this research work lies more in the integration of adaptive filtering techniques into a programmable CLTF module to serve as a complementary signal pulse for waveform modification in order to improve interference mitigation in higher frequencies. The fundamental innovation in combining these windowing techniques in a Closed-Loop Transfer Function (CLTF) module paired in a Hanning-induced Filtered-OFDM (F-OFDM) model is in achieving adaptive, real-time control over spectrum leakage while maintaining strict orthogonality and effectively balancing high spectral efficiency with robust asynchronization for 5G/6G systems. To the best of our knowledge, this gap has not been effectively addressed in previous research conducted relative to this area. Research has proven that a waveform cannot be created but can only be modified to meet peculiar needs.

II. THEORETICAL BACKGROUND

This Section expresses the theoretical background of this research work, which encompasses the filters' design and its realization. This has also presented the conceptual framework used for the formation of the alternative waveforms for AIM and the signal decision threshold. The filter design approach adopted is the windowing method. This is because signal filtering and windowing are two of the key criteria and performance tools required for waveform modification in the 5G NR system [1]. In this work, it is achieved using a CLTF module incorporated in an F-OFDM waveform. The CLTF module adopted in this work is a programmable memory system, having first-hand knowledge and the ability to autonomously adjust its received signal information in conformity with the transmitted signal information.

The Hanning, Kaiser, and Dolph windows are favorites in the design of the FIR filters in this research work. This is for the purpose of achieving effective control over spectral leakage, outrageous power, Doppler shift, frequency selectivity, extraneous power consumption, and filter tail distortions. Additionally, the Kaiser-driven and Dolph-induced filters are adjustable filters placed at the feedback region of a CLTF module incorporated in a Hanning-induced F-OFDM receiver. These induced filters serve as antidotes for AIM as required for modern-day wireless resource users [17]. With this systematic arrangement and timing, it generates an alternative signal waveform that is capable of mitigating all kinds of interferences to achieve effective system efficiency in a wireless network system.

A. Hanning Windowing Filter

The Hanning window is one of the most favorite and commonly used windows for sub-band filtering to achieve asynchronous waveforms. It belongs to a family of general cosine windows [19]. It has the advantage of generating lower side lobes, which helps in mitigating Out-of-Band Emission (OoBE) and Peak-to-Average Power Ratio (PAPR) in orthogonal systems [20]. This makes it a suitable candidate to be deployed at the head of a transmitter and tail of a receiver of a communication transducer. For this reason, it is used in the work to generate an F-OFDM asynchronous waveform that is subjected to AIM. Equation (1) is the expression for the HW co-efficient as computed in [21]:

$$W_{HW}^{*}(n) = 0.5[1 - \cos\left(\frac{2\pi n}{N_W}\right)]^{\alpha} \quad (1)$$

where, $N_W = M_f - 1$, that is the length of the window and α is the roll-off factor or the window shaping coefficient.

To obtain a HW induced FIR filter, $F_{HW}^{*}(n)$ for effective F-OFDM head/tail filtering, an ideal low pass filter sinc transfer function, $h_d(n)$ is multiplied with the HW function, $W_{HW}^{*}(n)$, as in [22]:

$$F_{HW}^{*}(n) = h_d(n)W_{HW}^{*}(n) \quad (2)$$

The F-OFDM received signal waveform is matched with the transmitted signal using convolutional matrix in time domain to obtain an asynchronous waveform, $R_{in}(n)$ in (3):

$$R_{in}(n) = R(s)^* F_{HW}^*(-n) \tag{3}$$

where, $R(s)^*$ is the received signal impulse response across subcarriers and $F_{HW}^*(-n)$ represent the folded version of the spectrum shaping FIR filter positioned at the receiver tail.

B. Kaiser Windowing Filter

The reason why Kaiser Window and FIR filters are employed in most current waveform study is to serve as enabler in controlling of spectral leakage, and to solve the problem of spectral concentration [23]. In the case of samples with N_W points, (4) defines the KW function, $W_{KW}^*(n)$ with an attenuation function, β. Equations (4) through (8) are used in computing the coefficients of a KW.

The KW equation is given for $0 \leq n \leq M_f = 1$ in [22], in correspondence to the filter taps, N_f:

$$W_{KW}^*(n) = \frac{lo[\beta\sqrt{1-\left(1-\frac{2n}{N_W}-1\right)^2}]}{lo[\beta]}, \tag{4}$$

where: $\beta = \pi\alpha$ is the attenuation function (consisting of the waveform phase, π and the roll-off factor, α) and $lo[.]$ is the modified zero-order Bessel function given in [24] as:

$$lo[\beta] = 1 + \sum_{k=1}^{\infty}[\frac{(\beta/2)^2}{k!}] \tag{5}$$

and,

$$\beta = \begin{cases} 0.1102(A_s - 8.7), & A_s \geq 50 \\ 0.5842(A_s - 21)^{0.3} + 0.07886(A_s - 21), & 21 < A_s < 50 \end{cases} \tag{6}$$

where, A_s is the minimum stop-band attenuation and β is the parameter that depends on N_W, and is chosen to yield various transition widths and near optimum stop-band attenuation. The pertinent design parameters are: w_s and A_s, which are obtained from the following relationships of the normal transition width [25]:

$$\Delta_{\omega} = \frac{w_s - w_p}{2\pi} \tag{7}$$

where, $w_s - w_p$ is the width of the transition band, with w_s denoting the width of the stop-band and w_p representing the width of the pass-band. w_s and w_p are also termed corner frequencies.

The filter length, $N_f = M_f - 1$ is also determined by selecting the lowest odd value of N_f that would satisfy the inequality [26]:

$$N_f \geq \frac{\omega_{\text{samp}} D}{\Delta\omega} + 1 \tag{8}$$

where the parameter D, is determined using the expression:

$$D = \begin{cases} 0.9222, & A_s \leq 21 \\ \frac{A_s - 7.95}{14.36\Delta f}, & A_s > 21 \end{cases} \tag{9}$$

and, ω_{samp} is the normalized sampling frequency and $\Delta\omega$ is the transition width.

However, windows are analyzed in the frequency domain in order to easily compare and classify them in terms of their spectral characteristics. The frequency spectrum of a window is obtained in (10):

$$W(e^{jwt}) = e^{-jw(N_W-1)T/2} W_0(e^{jwT}) \tag{10}$$

where,

$W_0(e^{jwT})$ is the amplitude function.
$N_W = M_f - 1$ denotes the window length, which is the same with the filter length, N_f used.
T corresponds to the interval between samples.

This is useful when plotting the normalized amplitude spectrum of the window.

To obtain the required attenuated waveform, the $F_{KW}^*(n)$ induced FIR window function is modulated with an F-OFDM signal that is mixed with ACI, ICI, and ISI, in order to filter out the interference signal pulses from the useful ones. Its corresponding filtered signal, $R_{KW}(n)$ is gotten in (11).

$$R_{KW}(n) = Z_n(n)^* F_{KW}^*(n) \tag{11}$$

where, $F_{KW}^*(n)$ is the FIR filtered signal that is obtained by the multiplication of an ideal low pass filter transfer function, $h_d(n)$ with KW functions, $W_{KW}^*(n)$ and $Z_2(n)$ represents the undesired F-OFDM signal that are contaminated with ACI, ICI, and ISI.

C. Dolph-Chebyshev Windowing Filter

The ability to produce wide main lobes (wideband) and effective control over spectral aliasing are some of the antecedents of DW. The zero-phase DW function, $W_{DW}^*(n)$ expressed in (12) is usually defined in terms of its real-valued discrete Fourier transform for $0 \leq n \leq M_f - 1$ [23].

$$W_{DW}^*(n) = \frac{\cos(N\cos^{-1}[\beta\cos(\frac{\pi k}{N_W})])}{\cosh[N\cosh^{-1}(\beta)]}, \tag{12}$$

$$\text{where, } \beta = \cosh[\frac{1}{N}cosh^{-1}(10^{\alpha})], \tag{13}$$

The value of α determines and influences the side-lobes attenuation. Its normal window function, $w_0(n)$ is presented in (14) as in [19].

$$w_0(n) = w_0(n - \frac{N_W}{2}), \tag{14}$$

Similar to (11), the $F_{DW}^*(n)$ induced window function is modulated with an F-OFDM signal that is distorted with ACI, ICI, and ISI, in order to separate these unwanted signals from the wanted ones. Its associated filtered signal, R_{DW}(n) is obtained in (15).

$$R_{DCW}(n) = Z_2(n)^* F_{DW}^*(n) \tag{15}$$

where, $F_{DW}^*(n)$ is the FIR filter that is obtained by the multiplication of an ideal low pass filter transfer function, $h_d(n)$ with DW functions, $W_{DW}^*(n)$.

III. RESEARCH METHODOLOGY

This section explicitly presents the materials and methods as well as the pictorial and mathematical models used in actualizing this research. The workability of the programmable CLTF module that enhances the signal waveform modification to achieve AIM is clearly demonstrated and interpreted. The developed module is incorporated at the receiver side of an F-OFDM wireless system in order to negotiate and complement signal bits that are distorted by interference or have defaulted from the transmission bits' standards. To achieve the required efficiency in the design, a seamless integration of the module and the wireless model that hosts the module is demonstrated using a flowchart algorithm.

A. Materials and Method

The materials that forms the successful integration of the CLTF model with the HW-OFDM system include the spectrum shaping filter folded version, G_1 the demultiplexer unit, $\otimes$ the channel estimation model, G_2 the error control system, β and the demodulator, $\otimes$. The following anecdotes are the research methods adopted as the working principles of the developed model of this work. Therefore:

- The received signal, $R_s(n)$ after passing through the fading channel is totalized and reconstructed at the receiver side of F-OFDM system.
- This received signal is prefiltered by a folded version of a spectrum shaping filter, G_1 to correct anomalies caused by channel noise and multipath echo.
- The demultiplexer unit, $\otimes$ cart-off the CP to remove network burden, where the system is noticed to reintroduced chunks of interference anomaly. These fragments of anomalies need to be mitigated in order to efficiently service higher 5G NR frequencies.
- The system gain region, G_2 is taken as the channel estimation region of the classification of anomalies, where a threshold of 0.5 is set within the bound of 0 and 1.
- This threshold is set to discriminate between signal that are defected by interference, $Z_2(n)$ and separate those with less interference, $Z_1(n)$.
- The defected signal, $Z_2(n)$ are extracted and referred to be postfiltered at the $H(n)$ *or* β region containing $F^*_{KW}(n)$ or $F^*_{DW}(n)$ filter. The $F^*_{KW}(n)$ and $F^*_{DW}(n)$ filters serve as complements in reforming the signal waveforms, $Z_2(n)$ in comparison to the transmission bits' standards.
- The filtered signal waveforms, $R_f(n)$ is reverted back to negotiate and compliment the received signal codes that are labelled interfered, which is certified via the system gain, G_2 to be demodulated.
- The final advanced alternative waveforms are achieved in the forms HKW-FOFDM and HDW-FOFDM systems.

B. System Modeling

Figure 1 presents a schematic workflow diagram of the methodology followed for the realization of a CLTF module built for the waveform modification. In this work, the HKW-FOFDM algorithm is employed to obtain both FR1/FR2 5G waveform requirements, whereas the DW-FOFDM is also used to achieve 5G FR2/FR-A waveform projections. This is aimed at meeting the International Telecommunication Union (ITU) and 3GPP NR release (15, 16, 17, and 18) requirement for waveform development.

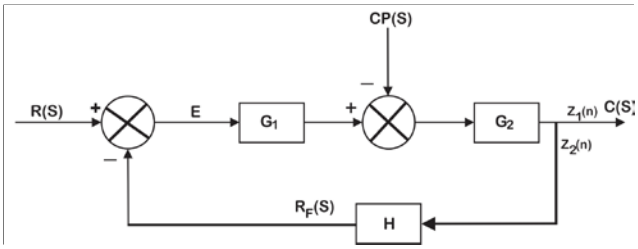

Fig. 1. A CLTF Feedback Module

The received signal response, $R(s)$ after passing through the offset channel is formulated in (16) as in [2]:

$$R_s(n) = [h(n)S(n) + W(n)] \tag{16}$$

where:

$h(n)$ represents the channel impulse response.
$S(n)$ means the F-OFDM information carrying symbols.
$W(n))$ is the Additive White Gaussian Noise (AWGN) channel which is a function of the type of fading channel experienced.

The waveform representation of (16) before the introduction of the folded version of the spectrum-shaping filter, takes the form:

$$y_k(n) = \frac{1}{K}\sum_{i=0}^{I}\sum_{n=0}^{N-1} R_k(n)e^{\frac{j2\pi}{N}} \tag{17}$$

where k is the waveform sample coefficient.

In the CLTF module of Fig. 1, G_1 represent the condition of the received signal information at the folded version of an asynchronous spectrum shaping filter, $F^*_{HW}(-n)$ of the F-OFDM system presented in (3). It is taken to be the same as the error factor regulator, E as:

$$G_1 = E = R_s(n) - R_f(n)Z_1(n) \tag{18}$$

where, $R_f(n)$ is the alternative filtered signals while $Z_1(n)$ corresponds to the CLTF baseband samples gained across the subcarriers.

To derive the CLTF gain, the *CP* burden in the channel estimation region, G_2 is first of all wart-off to increase system efficiency. This is seen demonstrated in the CLTF module in Fig. 1 as:

$$G_2 = G_1 - CP \tag{19}$$

Also, the alternative filtered signal response is derived as:

$$R_f(n) = H(n)Z_2(n) \tag{20}$$

Therefore, the conventional framework of the CLTF module for AIM signal waveform is modelled as:

$$\frac{Z_1(\mathrm{n})}{R_S(n)} = \frac{G_2}{1+G_2 R_f(\mathrm{n})} \quad (21)$$

Substituting (19) and (20) into (21), the baseband signal samples gain, $Z_1(n)$ across a wireless system yield:

$$Z_1(n) = \frac{[G_1 - \mathrm{CP}]R_S(n)}{1+[G_1 - \mathrm{CP}]R_f(\mathrm{n})} \quad (22)$$

$R_f(n)$ refiltered signals are either of $R_{KW}(n)$ or $R_{DW}(n)$, which are the alternative filtered signals generated in (11) and (15).

Therefore, the CLTF baseband samples gain, $Z_{HKW}(\mathrm{n})$ concealing the payload and pilot data altered by (11) is realized as:

$$Z_{HKW}(\mathrm{n}) = \frac{[F^*_{HW}(-n) - \mathrm{CP}]R_S(n)}{1+[F^*_{HW}(-n) - \mathrm{CP}]R_{HKW}(\mathrm{n})} \quad (23)$$

Similarly, the CLTF baseband samples gain, $Z_{HDW}(\mathrm{n})$ encompassing the payload and pilot data altered by (15) is generated as:

$$Z_{HDW}(\mathrm{n}) = \frac{[F^*_{HW}(-n) - \mathrm{CP}]R_S(n)}{1+[F^*_{HW}(-n) - \mathrm{CP}]R_{HDW}(\mathrm{n})} \quad (24)$$

Both $Z_{HKW}(\mathrm{n})$ and $Z_{HDW}(\mathrm{n})$ are adaptive systems that can be adjusted or altered autonomously, which can be used for generic applications to meet certain waveform demands.

Equations (23) and (24) are the seamless computation iterations taking place at the channel estimation region of the AIM model receiver. The AIM desired signal, after passing through these iterations, is demodulated to extract the original information.

Finally, the expected waveform equivalent of (23) and (24) at the receiver's output is presented in (25). It is achieved by converting (23) and (24) into their original orthogonally placed multicarrier nature, which is also a factor of the system numerology as required by 5G NR, yielding:

$$Y_K(e^{j\omega}) = \frac{K}{A_K}\int_{i=o}^{I}\int_{n=0}^{N-1} Z_k(e^{j\omega})e^{-\frac{j\omega}{N}} \quad (25)$$

where, Z_k is the modified AIM signal presented in (23) and (24)

IV. RESEARCH ALGORITHM

This section presents the graphical algorithm of a sub-band network architecture as considered in this research. This work derived an algorithm that compensates for the aberrations and signal broadcasting bottlenecks mostly noticed at the receiver side of the wireless system. Experimental works over time have proven that these bottlenecks experienced at the receiver side are caused by ACI, ICI, and ISI distortions. The process adopted for the compensation of defective transmission signal pulses is illustrated in Fig. 2.

Starting from the initialization of the input waveform data, which is in the time domain and to the output data, $y_k(n)$ which is in the frequency domain, $Y_K(e^{j\omega})$; the algorithm is scoped. After passing through the processes of modulation and multiplexing, the CP is removed to mitigate bandwidth wastage and relegate redundancies. In a sub-band architecture of this nature, ACI, ICI, and ISI distortions are seen to be more negatively impactful on the system after carting away the CP burdens.

The CLTF module is a programmable model, hosting the command to differentiate between pilot and payload data and wanted and unwanted signal pulses based on an established threshold of 0.5 between 0 and 1. The data classification is defined by considering 8-bit data/symbols driven by a 256 QAM mapping scale. The decision box in Fig. 2 serves as the channel estimation region, where the classification of the wanted and unwanted signal pulses is defined. By dividing the 8-bit data into two sets of nibbles (4-bit each), any data sample observed to have equal 0s and 1s is tagged as pilot data, where having more 0s than 1s in any symbol depicts wanted pulses and having more 1s than 0s connotes an unwanted scenario. In the situation where more 1s are noticed, the system activates its causality adaptability of prior information of the transmission pulses by comparing and compensating for the discrepancy; otherwise, it transmits "wanted."

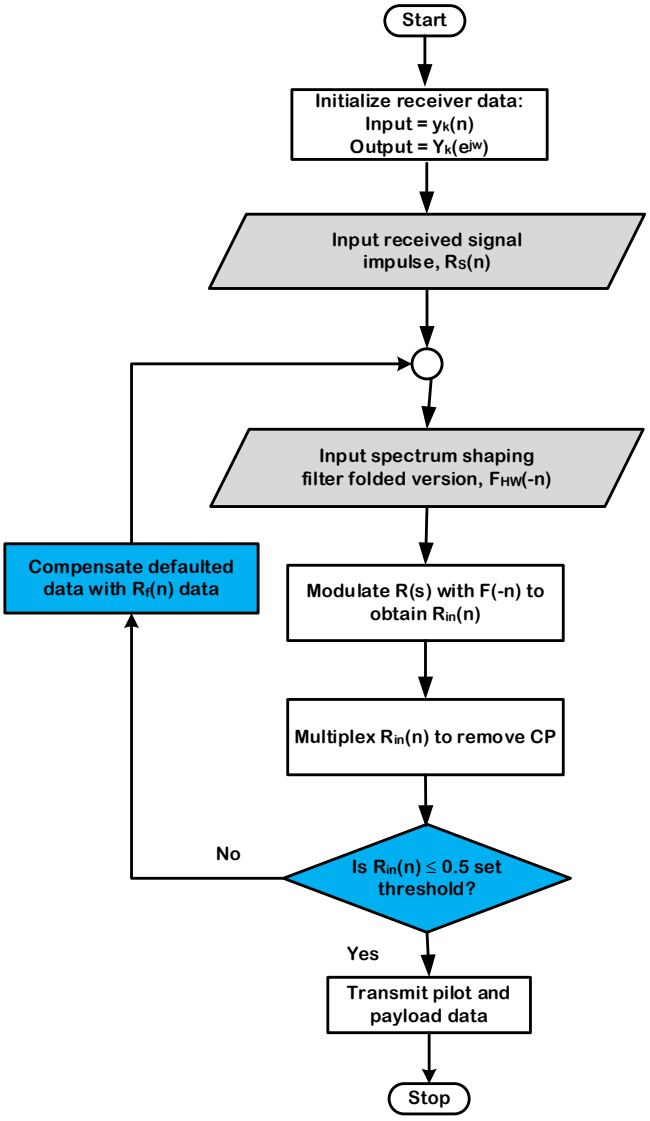

Fig. 2. AIM Flow Chart

V. RESULTS AND DISCUSSION

The simulations in this research are carried out using PyCharm IDE of Python scripts. The research considered $(1/16)N$ of CP size, where N is the IFFT/FFT length. A 257

filter length, N_f is considered in all cases. The window length, N_W is taken the same as the filter length, N_f. The adjustable characteristics of the two windowed filters (KW and DW) endorsed in this work, makes it possible to be varied to service the $15\ kHz\ x\ 2^n$ numerologies models as required to drive 3GPP 5G NR resources. This is for the purpose of achieving effective interference control that would improve the system processing time, increase data rate, achieve scalable throughput, and improve bandwidth optimization. The simulations carried-out here are within the confines of $60\ kHz$ and $120\ kHz$ Subcarrier Spacing (SCS) to achieve effective handover between 5G FR1 and FR2.

Each F-OFDM subcarrier symbol contains 8-bits data size, denoted in zeros (0) and ones (1). The data is expressed as wanted if there are more zeros than ones in the $8-bits$ class and unwanted if it contains more ones than zeros. In the event a subcarrier containing $4-bits$ of zeros and $4-bits$ of ones, it is termed a pilot subcarrier. The research also considered a data threshold of 0.5 within the bounds of the 0 and 1. Table 1 presents the summary of the remaining parameters used for this work.

Table 1
Research Parameters

Parameters	Specifications
Channel Access	F-OFDM
Filter mode	FIR
Window	Hanning, Kaiser, Dolf
Roll-off factor, α	1 for Hanning, variable from 0 to 10 for the adjustable windows.
β	1, 6, 10, 16
ρ	1, -45, -80, -100
FFT size, N	4096
Defected subcarriers, N_d	2016
Number of sub-bands, K	80
Defected Sub-bands,	42
Sub-band bandwidth, M	48
Bits per symbol	8
Bandwidth, BW	100 MHz, 200 MHz
Subcarrier spacing	60 kHz. 120 kHz
Service Numerology	2, 3
Mapping order	256 QAM

A. Hann, Dolph, and Kaiser Windows Induced Filters Frequency Responses

This Section presents results obtained from individual frequency responses of Hann, Dolph, and Kaiser induced filters in dBm. As presented in the analyses, the final results would be obtained in the categories of Hann-Kaiser Windowed (HKW) and Hanh-Dolph Windowed (HDW) induced FIR filters responses/gains, in comparison with the individual Hann Windowed (HW) induced filter response in terms of interference mitigation. In wireless communication having an IFFT/FFT data size of 4096 symbols in the multiple of $8-bits$ each is quite a huge data set assigned for 5G systems. Due to limitation in equipment, the data size is sub-divided into 48 sub-bands bandwidth in the multiple of $8-bits$ each then superimposed into 12 subcarriers index samples. To compute this dada size at once would results to complex analysis. In this light, the data are categorized into; $(1)\ 0-47, (2)\ 48-95, \ldots, (80)\ 4067-4095$. The analysis considered the reference (1) data class as the most vulnerable, capable of experiencing interference aberrations more than any other classes.

Figure 3, is the frequency response of Hann Windowed filter, $F^*_{HW}(n)$. Its roll-off factor is taken as 1 in this work. The result shows Hann induced window exhibiting fewer side lobes at -45 dBm. This makes this filter very effective in spectral leakages control of Out-of-Bound Emission and Peak-to-Average Power Ratio (PAPR). With this quality milestone, the Hann Widowed filter is suitable for deployment at the head/tail regions of a wireless waveform. In this work, it is obtained within the context of $120\ kHz$ SCS having an inbuilt Hanning induced FIR system with 257 tappers.

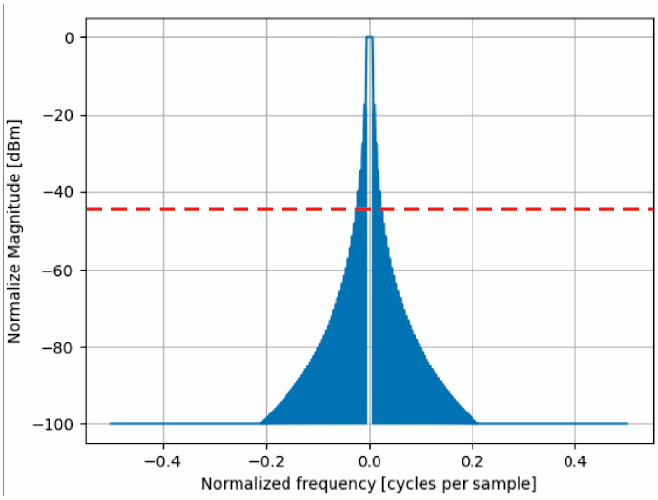

Fig. 3. Frequency Response of Hann-Induced FIR Filters

Figures 4 (a & b) presents the individual frequency responses of Kaiser induced and Dolph induced FIR filters. It is observed that Kaiser at $\beta = 6$ performs almost equal to Dolph at $-45\ dBm$. The attenuation function, β and the pass-band ripple factor, ρ parameters are continuously varied to obtain the desired FIR filter that aids in achieving alternative waveforms used for AIM and for noise control within the likelihood of emitting interference. Results obtained show the Kaiser-induced filter obtained a small main lobe width with high steepness, which is good in controlling main lobe width friction. The Dolph-induced filter is seen having its main lobe width as the widest. The Dolph is noted to generate greater performance with respect to stop-band attenuation, recording higher noise reduction capability than others but less steepness.

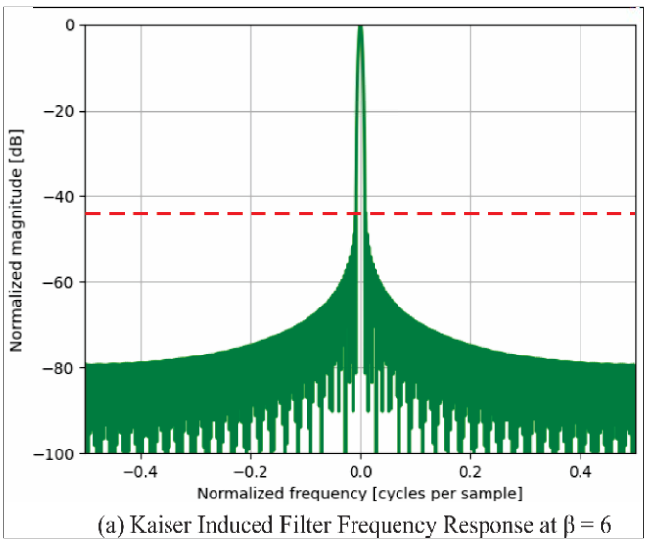

(a) Kaiser Induced Filter Frequency Response at β = 6

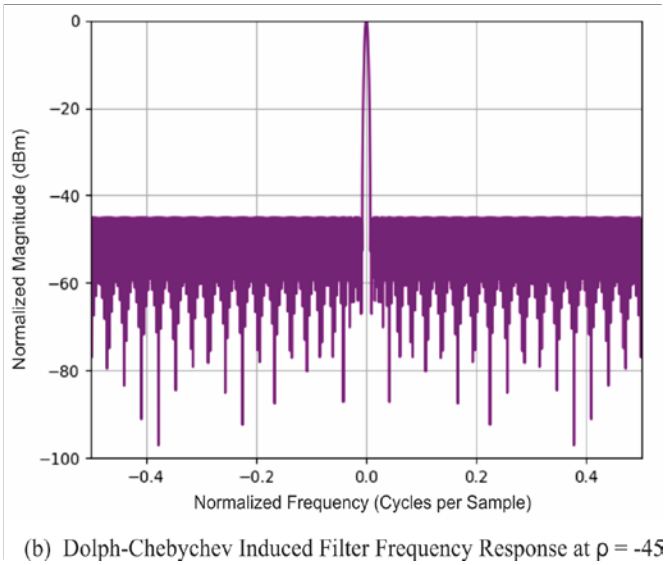

Fig. 4. Frequency Response of Kaiser and Dolph Induced FIR Filters

B. Interference Mitigation Results

In order to avoid complication in the simulation and readings, this research presented its results using the mathematical model of a baseline value. The sample data are synthesized by the superposition of the 48 sub-band bandwidths into 4 bands to obtain 12-sample index each. The average AIM power, I_{AIM} and baseline values, I_{BV} are determined using the summation of individuals' power, I_{Total} divided by the number of sample index, I_{Samp} as:

$$I_{AIM/BV} = \frac{\sum_{k=1}^{M} I_{Total}}{I_{Samp}} \quad (26)$$

The Performance Improvement (PI) of the developed HKW-FOFDM and HDW-FOFDM models are compared with the conventional HW-FOFDM technique for the AIM analysis and are presented in percentage in terms of ICI, ISI, and ACI mitigation, as in (27):

$$PI = \frac{I_{AIM} - I_{BV}}{I_{BV}} \; x \; 100\% \quad (27)$$

Figure 5 juxtaposes simulation results obtained for interference power mitigation of ACI, ISI, and ICI using HW induced F-OFDM waveform with varied SCS. The interfered waveforms are keenly observed and estimated after the CP removal. The same CP length is chosen for 60 kHz SCS and for 120 kHz SCS for 5G NR transmission for the purpose of comparing the system scalability. It is obvious that the ICI sensitivity of -41.79 dBm achieved at for 120 kHz SCS has better interference mitigation than all indexes, in which ACI sensitivity of -20.55 dBm is viewed to be worst in all results and more aggravated at 60 kHz SCS with -16.95 dBm. This is because of the correlation between SCS rate and CP length. At 120 kHz SCS, the average ACI level at -20.55 dBm proved to be more impactful by obtaining 21.23% compared to its baseline value. This is better than those obtained from ISI at -32.08 dBm and ICI at -41.79 dBm, due to effective asynchronicity among the sub-bands. Likewise, it is viewed that ISI shows more impact on the system than ICI.

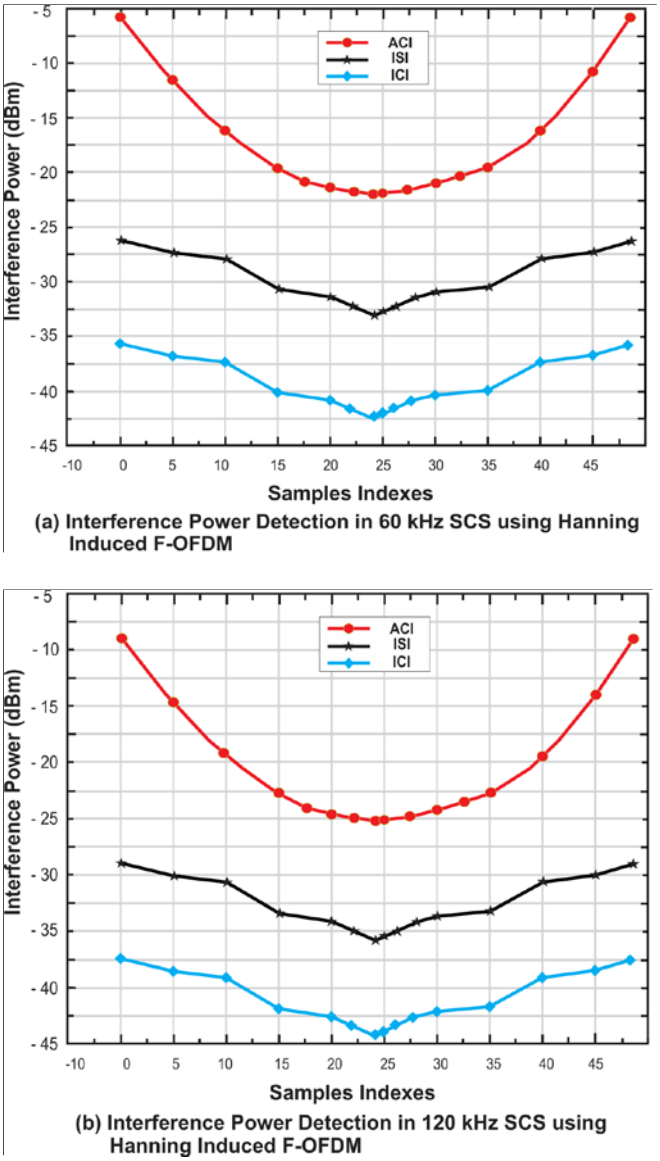

Fig. 5. Hanning induced F-OFDM Interference Power Mitigation with Subcarrier Bandwidth, $M = 48$ at (a) $\Delta_f = 60$ kHz and (b) $\Delta_f = 120$ kHz.

Table 2 present the comparison of interference mitigation at 60 kHz SCS and 120 kHz SCS of HW induced filter. It is observed that the HW-FOFDM system at 120 kHz obtained interference control of -20.55 dBm for ACI, -32.08 dBm for ISI, and $-41,79$ dBm for ICI better than that obtained at 60 kHz SCS: with -16.95 dBm for ACI, -29.45 dBm for ISI, and -39.25 dBm for ICI. Consequently, the HW-F-OFDM at 120 kHz SCS obtained an improvement of 21.23% for ACI, 8.93% for ISI, and 6.47% for ICI over that at 60 kHz SCS. However, it is observed from the result presented in dBm, that the interference power does meet up the estimated threshold of 50 dBm to 120 dBm designated for effective 5G FR2 transmission, as such can only transmit FR1 frequencies. This has clearly shown the limitation of HW induced FOFDM systems in terms of system scalability. Furthermore, is observed that the HW-FOFDM performance at 120 kHz SCS degrades with every increase in data compared to its performance at 60 kHz. This simply means that the HW induced F-OFDM does not drive above 5G FR1 requirements, which led to the conception of the idea for the

development of an AIM model in this research, with the sole capability to drive above the 5G FR1 objectives.

Table 2
Interference Power Mitigation of HW-OFDM at 120 kHz versus 60 kHz SCS

Interference	HW-OFDM at 60 kHz SCS	HW-OFDM at 120 kHz SCS	Percentage Improvement
ACI Power (dBm)	-16.95	-20.55	21.23%
ISI Power (dBm)	-29.45	-32.08	8.93%
ICI Power (dBm)	-39.25	-41.79	6.47%

Figures 6 and 7 respectively show pictorial results obtained from simulations for AIM at 120 kHz SCS using Hann-Kaiser Windowed (HKW) and Hann-Dolph Windowed (HDW) induced filters interchangeably. It is observed from the results in both figures that HKW-FOFDM waveform produces better ICI and ISI mitigation at $-53.70\ dBm$ – and $-40.05\ dBm$ than HDW-FOFDM of $-51.17\ dBm$ and $-38.52\ dBm$, respectively. This is simply because the Kaiser windowed induced FIR filter has better interference cancellation capability to a bearable level by virtue of its optimal control on the spectral leakage and also its merits on spectral concentration than Dolph windowed induced FIR filter. On the other hand, the HDW-FOFDM waveform gives the best waveform in terms of ACI mitigation at -30.02 dBm better than HKW-FOFDM which achieved $-25.22\ dBm$. ACI effect is associated with noise and it mostly transpires at the surface of the subcarriers of the system.

When the interference mitigation capability of the newly developed HKW-FOFDM model at 120 kHz SCS was compared with those achieved using HW-FOFDM system, as demonstrated in Table 3. It is seen that the HKW induced F-OFDM system outperformed the traditional HW induced F-OFDM system used in driving 5G FR1. The HKW-FOFDM achieved an average interference power control of $-25.22\ dBm$ for ACI, $-40.05\ dBm$ for ISI, and $-53.70\ dBm$ for ICI better than those achieved in HW-FOFDM system of $-20.55\ dBm$ for ACI, $-32.08\ dBm$ for ISI, $-41.79\ dBm$ for ICI. The HKW-FOFDM system also achieved an interference improvement of 22.72% for ACI, 24.84% for ISI, and 28.49% for ICI over the conventional HW-FOFDM system.

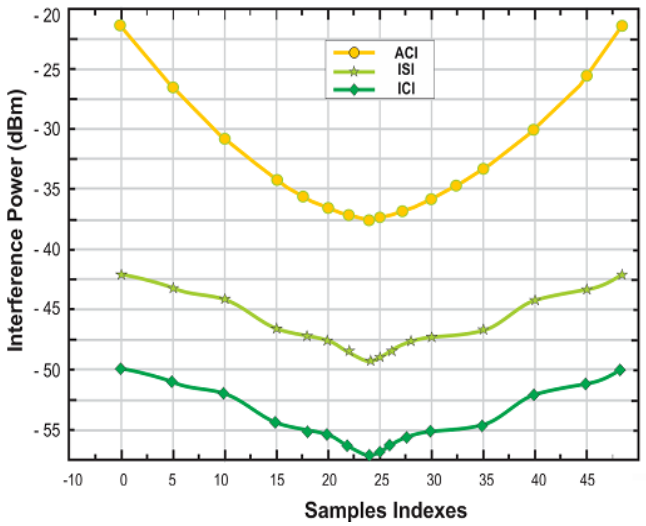

Fig. 6. Interference Power Mitigation of HKW-FOFDM Induced FIR Filters at 120 kHz SCS.

Table 3
Interference Power Mitigation of HKW-OFDM at 120 kHz versus HW-OFDM 120 kHz SCS.

Interference	HW-OFDM at 120 kHz SCS	HKW-OFDM at 120 kHz SCS	Percentage Improvement
ACI Power (dBm)	-20.55	-25.22	22.73%
ISI Power (dBm)	-32.08	-40.05	24.84%
ICI Power (dBm)	-41.79	-53.70	28.49%

Similarly, Figure 7 and Table 4 present the interference mitigation capability of HDW-FOFDM system against those obtained in HW-FOFDM system at 120 kHz SCS. Results obtained show the HDW induced F-OFDM achieved interference control of $-30.02\ dBm$ for ACI, $-38.52\ dBm$ for ISI, and $-51.17\ dBm$ for ICI better than $-20.55\ dBm$ for ACI, $-32.08\ dBm$ for ISI, and $-41.79\ dBm$ for ICI achieved by HW induced F-OFDM system. Furthermore, the HDW-FOFDM also achieved improvement over the HW-FOFDM by 46.08% for ACI control, 20.07% for ISI, and 22.44% for ICI. Considering the variation in interference mitigation, shows that the HDW-FOFDM mitigates ACI better than the HW-FOFDM and HKW-FOFDM systems. This simply means that the HDW-FOFDM is good model for the generation of asynchronous systems.

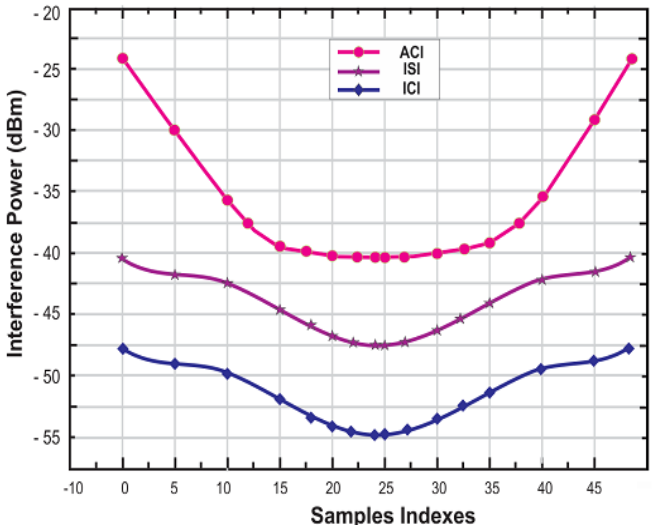

Fig. 7. Interference Power Mitigation of HDW-FOFDM Induced FIR Filters at 120 kHz SCS.

Table 4
Interference Power Mitigation of HDW-OFDM at 120 kHz versus HW-OFDM 120 kHz SCS

Interference	HW-OFDM at 120 kHz SCS	HDW-OFDM at 120 kHz SCS	Percentage Improvement
ACI Power (dBm)	-20.55	-30.02	46.08%
ISI Power (dBm)	-32.08	-38.52	20.07%
ICI Power (dBm)	-41.79	-51.17	22.44%

Comparing Figures 6 and 7 with the interference power result obtained in Fig. 5 (b), show that HKW and HDW filters induced FOFDM waveforms mitigates interference better than individual HW induced FOFDM. In like manner, it was viewed that the HKW and HDW induced FOFDM increases the system scalability whenever SCS and β are varied upward. Furthermore, the HKW AIM waveform enabler produce signals which suited the requirement for effective orthogonality and the HDW enabler AIM waveform has assure an effective asynchronous signal. Finally, waveforms obtained from HKW and HCW filtering in Fig. 6 and 7 are

passed through a demodulator using an FFT operator to produce the newly developed alternative waveform that falls within the AIM requirement for 5G NR FR2 systems.

VI. CONCLUSION AND RECOMMENDATION

In conclusion, this work achieved an AIM transmission efficacy using HKW-FOFDM and HDW-FOFDM models in a CLTF module of an augmented filtering approach. Results achieved show that the two developed simultaneous models outperformed the conventional HW-FOFDM system in terms of interference mitigation by enabling effective 5G FR2 transmission. The HKW-FOFDM generated the highest ICI and ISI values, therefore enabling an effective orthogonal system. The HDW-FOFDM also produces better ACI values that depict safer asynchronous systems. At 120 kHz SCS, both HKW and HDW induced systems perform better the traditional method of HW-induced F-OFDM. The models are implemented using windowing with a non-recursive structure. This is because windowing and filtering of the traditional multicarrier waveforms is one of the requirements for designing highly flexible waveforms for the 5G NR networks and beyond. In addition, they can easily be designed and also be implemented in cyclic waveforms because the response of the filter depends only on the present and past input samples (causality). At the core of the work, the newly developed models seamlessly solved constraints that have to do with fundamental problems earlier noticed from the multicarrier OFDM design, including structural, numerical, and physical modeling, particularly within the FR2 range. This has informed one of the reasons for the conception of the non-non-unity CLTF module, which is intended to correct these fundamental problems of high OoBE suppression and PAPR.

Among the areas that require further work are these recommendations:

i. The hybridization of HKW-FOFDM and HDW-FOFDM waveforms can provide better alternative and adaptive stop-band attenuation, high steepness, shallow side lobes, and higher noise reduction. This is because it will combine all the advantages of Hanning, Kaiser Windows, and Dolph Windows but is detrimental to increasing power consumption. Future research can be conducted on how to mitigate this excessive power consumption in a hybridized system of this algorithm in order to further improve 5G NR wireless system efficiency.

ii. This research has not been able to achieve its simulations above 120 kHz SCS. This is a result of hardware constraints that resulted in difficulty in data iterations encountered in the course of trying to run simulations above 120 kHz. This has clearly proved the need for supercomputer systems of higher generations in order to increase system efficacy that could warrant an effective iteration of higher SCS.

iii. It is analytically and computationally observed that higher SCS at 120 kHz SCS mitigates interference and increases data rate but has also been noticed to introduce network redundancies in every increase in SCS. With these limitations, there may be a need for an improvised technique for the effective utilization of these unused spectra. The hybridization of Software Defined Radio (SDR) and Machine Learning (ML) algorithms may maximize the utilization of these redundant spectra and improve system scalability.

ACKNOWLEDGMENT

The authors wish to acknowledge the Air Force Institute of Technology Kaduna and the Federal University of Applied Sciences Kachia for providing the enabling environments and facilities for the conduct of this research.

CONFLICT OF INTEREST

The authors declare that there is no conflict of interest regarding the publication of the paper.

AUTHOR CONTRIBUTION

All authors contributed equally to the conception and design of the study, data collection and testing, analysis, and manuscript preparation.

REFERENCES

[1] F. Conceição, M. Gomes, V. Silva, R. Dinis, A. Silva, and D. Castanheira, “A Survey of Candidate Waveforms for beyond 5G Systems,” *Electronics*, vol. 10, no. 1, p. 21, Dec. 2020, https://doi.org/10.3390/electronics10010021

[2] Z. Augustine, A. M. Tekanyi, S. M. Sani, A. D. Usman, A. S. Yaro, “Development of a Novel Feedback Filtered Orthogonal Frequency Division Multiplexing Scheme for 5G Network and Beyond,” *Journal of Telecommunication, Electronic and Computer Engineering (JTEC)*, vol. 13, no. 4, pp. 1-6, Dec. 2021.

[3] R. Priya and R.K Budania, "Innovative Multi-Band Switchable Microwave Filter for Future Wireless Communication Systems." *Cuestiones de Fisioterapia* 54.3 (2025): 5248-5254.

[4] L. Zhang, A. Ijaz, P. Xiao, M. M. Molu, and R. Tafazolli, “Filtered OFDM systems, algorithms, and performance analysis for 5G and beyond,” *IEEE Transactions on Communications*, vol. 66, no. 3, pp. 1205–1218, Nov. 2017, https://doi.org/10.1109/tcomm.2017.2771242

[5] H. A. Marzog, H. J. Abd and A. Z. Yonis, "Noise Removal of ECG signal using Multi-Techniques," *2022 IEEE Integrated STEM Education Conference (ISEC)*, Princeton, NJ, USA, 2022, pp. 397-403, https://doi.org/10.1109/ISEC54952.2022.10025094

[6] G. Chandra, N. Sahu, R. Sahu, and P. K. Rahi. “Design of Low Pass FIR Filter Using Parzen and Nuttall Window Techniques,” *International Journal for Research in Emerging Science and Technology*, vol. 3, no. 8, pp. 11-16, 2016.

[7] A. Z. Yonis and K. K. Mohammed, “Investigation of pattern division multiple access technique in wireless communication networks Indonesian,” *Journal of Electrical Engineering and Computer Science* vol. 26, no. 1, April 2022, pp. 296-303. http://doi.org/10.11591/ijeecs.v26.i1.pp296-303

[8] A. Andrawes, R. Nordin, and N. F. Abdullah, “Energy-Efficient Downlink for Non-Orthogonal Multiple Access with SWIPT under Constrained Throughput,” Energies, vol. 13, no. 1, p. 107. 2020. https://doi.org/10.3390/en13010107

[9] Z. Augustine, H. Bello, A. M. S. Tekanyi, A. S. Yaro, H. A. Abdulkareem, O. O. Umeonwuka, U. F. Abdu-Aguye, “Generation of 5G frequency one model based on orthogonal multiple access technique of filtered-orthogonal frequency division multiplexing scheme for advanced interference evaluation,” Computers and Electrical Engineering, vol. 128, pp. 110056. Jan. 2025, 1;123:110056.

[10] H. Hong and Z. Li, “Hybrid Adaptive Bias OFDM-Based IM/DD Visible Light Communication System,” *Photonics*, vol. 8, no. 7, p. 257, Jul. 2021, https://doi.org/10.3390/photonics8070257

[11] P. Achimugu, Z. Augustine, M.J. Abdullahi, O. Lanihu, R.E. Yoro, A.A. Abba, and A. Hamisu, “A Survey of Wireless Cellular Network Generations and Their Channel Access Techniques” *Journal of Computing and Social Informatics* Vol. 5, No. 1, 2026, pp. 1-12. https://doi.org/10.64509/jicn.21.50

[12] A. Kumar and N. P, “OFDM system with cyclostationary feature detection spectrum sensing,” *ICT Express*, vol. 5, no. 1, pp. 21–25, Feb. 2018, https://doi.org/10.1016/j.icte.2018.01.007

[13] S. Natarajan, S.K. Mani, "OFDM implementation of image and video capturing with SD Ram using Artix-7." *AIP conference proceedings*. Vol. 2857. No. 1. AIP Publishing LLC, 2023. https://doi.org/10.1063/5.0165360

[14] Z. Augustine, A.S. Yaro, A.M.S. Tekanyi, H Bello, U.F. Abdu-Aguye, and EE Agbo,. "Feedback filtered-OFDM waveform candidature for interference mitigation in 5G networks and beyond." *International Journal of Integrated Engineering* Vol. 17, No. 1, 2025, pp. 323-339. https://doi.org/10.30880/ijie.2025.17.01.027

[15] J. Bai, S. Yuan, Z. Duan. "Research on the Interference Effects of 5G's Key Parameters on Radio Altimeters," *Aerospace* **2025**, vol. 12, p. 16. https://doi.org/10.3390/aerospace12010016

[16] A. Boruah, N.H. Singh, A. Biswas, S. Majumder, "Enhancing 5G Data Transmission Through Sub-Carrier Spacing Optimization." *Engineering Access* 11.1 (2025): 24-44.

[17] D.T. Hieu, T. Van Nghia, and N. Le Cuong, "Window-based alternative filters for f-OFDM in next generation wireless communication systems." *Journal of Military Science and Technology* 87, pp. 9-19, 2023. https://doi.org/10.54939/1859-1043.j.mst.87.2023.9-19

[18] A. Andrawes, R. Nordin, and M. Ismail. "Wireless Energy Harvesting with Cooperative Relaying under the Best Relay Selection Scheme," *Energies*, vol. 12, no. 5, 892. https://doi.org/10.3390/en12050892

[19] H. Rakshit and M. A. Ullah, "A comparative study on window functions for designing efficient FIR filter," *2014 9th International Forum on Strategic Technology (IFOST)*, Cox's Bazar, Bangladesh, 2014, pp. 91-96, https://doi.org/10.1109/IFOST.2014.6991079

[20] Z. Augustine, U.F. Abdu-Aguye, A.S. Yaro, H. Bello, A.M.S. Tekanyi, O.O. Umeonwuka, I. Yau, "Wireless multi-carrier transmission techniques for commercial deployment in LTE, LTE-A, and 5G FR1." *Journal of Electrical Systems and Information Technology* 12.1 (2025): 77. https://doi.org/10.1186/s43067-025-00270-5

[21] S. Bhowmik, M. S. Jahadun-Nobi, R. Chowdhury, O. M. Ali, S. Chowdhury, and M. S. Boby. An Efficient Optimized Window Function for Designing Low Pass FIR Filter. *IOSR Journal of Electrical and Electronics Engineering*, vol. 15, no. 4. pp. 26-32, 2020. https://doi.org/10.9790/1676-1504012632

[22] M. Yang, Y. Chen and L. Du, "Interference Analysis and Filter Parameters Optimization for Uplink Asynchronous F-OFDM Systems," in *IEEE Access*, vol. 7, pp. 48356-48370, 2019, https://doi.org/10.1109/ACCESS.2019.2910592

[23] A. Hammoodi, L. Audah, L. Al-Jobouri, M. A. Mohammed, and M. S. Aljumaily, "New 5G Kaiser-Based windowing to reduce out of band emission," *Computers, Materials & Continua/Computers, Materials & Continua (Print)*, vol. 71, no. 2, pp. 2721–2738, Dec. 2021, https://doi.org/10.32604/cmc.2022.020091

[24] R. P. Narwaria and M. Kumar. "Comparison of FIR Filter Using Different Window Functions," *International Research Journal of Engineering and Techology* . vol. 05, no. 10, pp. 634-637, Oct. 2018.

[25] E. Punskaya. Design of FIR Filter, E. Punskaya. "Design of FIR Filter," University of Oxford, [Online]. Available: https://www.robots.ox.ac.uk/~gari/teaching/cdt/A3/readings/Filtering_and_FFT/3F3_5_Design_of_FIR_Filters.pdf, Accessed: Mar. 24, 2025

[26] H. N. Uzo, O. U. Oparaku, and V. C. Chijindu, "Design of FIR digital filters using Semi-ellipse window," *Indonesian Journal of Electrical Engineering and Informatics (IJEEI)*, vol. 9, no. 3, Sep. 2021, https://doi.org/10.52549/ijeei.v9i3.2481